Inorganic Chemistry

ARTICLE

pubs.acs.org/IC

Exploratory Syntheses and Structures of $SrAu_{4.3}In_{1.7}$ and $CaAg_{3.5}In_{1.9}$: Electron-Poor Intermetallics with Diversified Polyanionic Frameworks That Are Derived from the $CaAu_4In_2$ Approximant

Qisheng Lin and John D. Corbett*

Department of Chemistry, Iowa State University, Ames, Iowa 50011, United States

Supporting Information

ABSTRACT: The phase regions around quasicrystals and approximants (QC/ACs) are rich pools for electron-poor intermetallics with novel, complex structures, and bonding patterns. The present $SrAu_{4.30(1)}In_{1.70(1)}$ (**1**) and $CaAg_{3.54(1)}In_{1.88(1)}$ (**2**) were synthesized through chemical tunings of the model $CaAu_4In_2$ (YCd_6-Type) AC. Single crystal X-ray diffraction analyses reveals that crystal **1** has *Pnma* ($CeCu_6$-type) symmetry, with $a = 9.102(1)$ Å, $b = 5.6379(9)$ Å, and $c = 11.515(2)$ Å. The building block in **1** is a 19-vertex cluster $Sr@Au_9In_4M_6$ (M = Au/In), which vividly mimics $Ca@(Au,In)_{18}$ in $Ca_3Au_{12.4}In_{6.1}$ (YCd_6-type) in geometry. These clusters aggregate into one-dimensional columns extending along the *b* axis. Crystal **2** (*P6/mmm*, $a = 20.660(3)$ Å, $c = 9.410(2)$ Å) is closely related to $Na_{26}Cd_{141}$ (*hP*167) and $Y_{13}Pd_{40}Sn_{31}$ (*hP*168), which are differentiated by the selective occupation of Wyckoff 1*a* (0 0 0) or 2*d* (1/3 2/3 1/2) sites by Cd or Pd. Crystal **2** adopts the $Na_{26}Cd_{141}$ structure, but the 1*a* site is split into two partially occupied sites. The synergistic disorder in the hexagonal tunnels along *c* is a major property. The valence electron count per atom (*e*/*a*) values for **1** and **2** are 1.63 and 1.74, respectively, the lowest among any other ternary phases in each system. These values are close to those of ACs in the Ca−Au−M (M = Ga, In) systems. Electronic structures for both are discussed in terms of the results of TB-LMTO-ASA calculations.

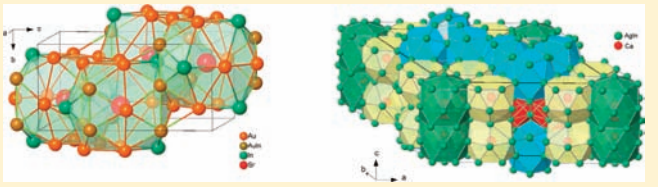

INTRODUCTION

Electron-poor intermetallics,[1] by which we mean those phases that have low valence electron counts per atom (e/a), namely, close to or lower than 2.0, have recently attracted considerable attention because of their close relationship to the Hume−Rothery phases (e/a < 2.0). The last phases originally refer to distinctive structural types (brasses) in the Cu−Zn binary system[2,3] but recently the more structurally complex quasicrystals and approximant phases (1.7−2.2), abbreviated as QC/ACs, have also been included in this category.[4] Electron-poor intermetallic phases are electronically positioned between the Hume−Rothery and the Zintl phases (e/a > 4.0).[5−7] (Note that the last values have traditionally been calculated for the anions only.) Generally, the metal−metal bonding interactions among electronegative constituents in polar intermetallics exhibit mainly covalent character, similar to the Hume−Rothery phases, but the interactions between electropositive metals and polyanions may also show considerable covalent bonding depending on the extent of electron transfer between them. Electron-poor intermetallics have been poorly investigated, and the interplays among valence electron count, structure, and bonding are not well understood.

Electron-poor polar intermetallics may be accessed by different routes. Besides decreases in the proportion of the alkali- or alkaline-earth metals, e/a values can also be decreased by alloying Zintl ions with electron-poorer transition metals,[1] for example, group 11 metals, Au particularly. Another good place to start is the phase regions around quasicrystals and approximants (QC/ACs).[5] According to our earlier experimental results, such electron-poor polar intermetallics may have complex structures, as do QC/ACs, and unprecedented structural units and novel bonding patterns. For example, $Sc_4Mg_{0.5}Cu_{14.5}Ga_{7.6}$ is a polar intermetallic phase exhibiting an incommensurately modulated structure, and its chemical composition and e/a are very close to those of the $Sc_3Mg_{0.2}Cu_{10.5}Ga_{7.3}$ 1/1 AC or $Sc_{15}Mg_3Cu_{48}Ga_{34}$ (= $Sc_3Mg_{0.6}Cu_{9.6}Ga_{6.8}$), the icosahedral QC.[8] Other parallel electron-poor intermetallics discovered in such ways include $Mg_{35}Cu_{24}Ga_{53}$,[9] $Ca_3Au_{10}In_4$,[10] and $Ca_3Au_8Ge_3$.[11]

During the past years, we have often utilized the combination of Ca and Au with other p-block elements in searches for QC/ACs, for example, Ca−Au−M (M = Ga,[12,13] In,[14] Ge,[15] Sn[16,17]). In addition, we have also considered chemical tunings in terms of both the active metal Ca and the dominant Au. It appears that the active metals Ca, Yb, and Y play critical roles in the formation of the YCd_6-type QC/ACs. On one hand, these metals have evidently suitable atomic sizes and electronegativities to match the electronegative components to meet the general conditions required by the Hume−Rothery rules.[2,3] On the other hand, they have low-lying empty or partially filled d valence orbitals to interact effectively with s and p states of electronegative components, through which the depths of pseudogaps around Fermi energies are greatly enhanced.

Received: July 28, 2011
Published: October 11, 2011

dx.doi.org/10.1021/ic2016275 | *Inorg. Chem.* 2011, 50, 11091–11098

For this reason, Na and Mg are evidently not suitable for YCd_6-type QC/ACs.[14] The heavier alkali or alkaline-earth metals have larger sizes and also contain empty d orbitals, but no QC/AC containing K, Rb, Cs, Sr, and Ba has been reported. Systematic experimental studies are very much needed. Another feature is the influence of the magic Au (with the largest relativistic effects among all metals) in the formation of QC/ACs. Au appears to be unique as the major component (>50 at. %) in the formation of Ca−Au−M QC/ACs (M = Ga,[12,13] In,[14] Ge,[15] Sn[16,17]) in terms of both electronic and size effects. The question as to whether Au is a required constituent is also interesting.

This work reports two different chemical tunings, $SrAu_xIn_{6-x}$ and $CaAg_yIn_{6-y}$, derived from the earlier studies on $CaAu_4M_2$ (M = Ga, In, Ge, Sn)[13−16] systems to test whether Ca or Au is required. Not surprisingly, each results in a new but not a YCd_6-type phase, although the starting compositions and reaction conditions were very similar to those employed to gain such products.

EXPERIMENTAL SECTION

Syntheses. The starting materials were calcium granules (99.5%, Alfa-Aesar), dendritic strontium (99.9%, Alfa-Aesar), gold foil (Ames Lab, > 99.99%), silver shot (Ames Lab, > 99.99%), and indium ingots (99.99%, Alfa-Aesar) that were stored in a glovebox filled with nitrogen (H_2O, < 1 ppmv). The surfaces of calcium, strontium, and indium metals were cleaned with a surgical blade before use. Mixtures were weld-sealed under an argon atmosphere into tantalum containers, which were later sealed within an evacuated SiO_2 jackets ($<10^{-5}$ Torr). Samples were heated to 850 °C, held at this temperature for 24 h, cooled to 500 °C at a rate of 2 °C/h, and annealed there for 3 weeks before being quenched in water.

Reactions with formula of $SrAu_xIn_{6-x}$ and $CaAg_yIn_{6-y}$ (x, y = 3, 4, 5) were designed because our similar studies on the $CaAu_xIn_{6-x}$ compositions had resulted in both QC and ACs.[14] However, both series yielded unexpected products instead. X-ray diffraction analyses revealed that what was refined to be $SrAu_{4.3}In_{1.7}$ (*Pnma*), compound **1**, was the major product of "$SrAu_4In_2$" (90 vol %) and "$SrAu_5In$" (~ 70%), whereas the nominal "$SrAu_3In_3$" produced mainly the known phase $SrAu_3In_3$ (*Pmmn*).[18] For the Ca series, the reflection peaks of "$CaAg_4In_2$" were completely indexed with the powder pattern simulated from single crystal data of $CaAg_{3.6}In_{1.9}$ (*P6/mmm*), compound **2**. The last was also the major product of "$CaAg_5In$" (~ 80%). In contrast, "$CaAg_3In_3$" yielded a pure product of 2/1 AC.[19]

After single crystal structures were determined, reactions with the refined elemental proportions for **1** and **2** were loaded again and reacted under the same reaction conditions. Both resulted in high yield products (c.f. Supporting Information, Figure S1), brittle with metallic lusters. Both products appear under low power microscopy to be air and moisture stable for years at room temperature. The average elemental proportions for **1** and **2**, measured via semiquantitative energy-dispersive X-ray spectroscopy (EDX) on a JEOL 840A scanning electron microscope (SEM), were Sr: Au: In = 1: 4.1(1): 1.9(1) and Ca: Ag: In = 1: 3.6(1): 1.9(1), respectively.

X-ray Diffraction. Phase analyses were based on powder X-ray diffraction data, which were collected on a Huber 670 Guinier powder camera equipped with an area detector and Cu Kα_1 radiation (λ = 1.540598 Å). The detection limit of a second phase with this instrument is conservatively estimated to be about 5 vol % in equivalent scattering power, so that an apparently single phase pattern is concluded to represent >95% phase purity.

Single-crystal X-ray diffraction data were collected at room temperature with the aid of a Bruker APEX CCD single crystal diffractometer equipped with graphite-monochromatized Mo Kα (λ = 0.71069 Å) radiation, and with exposure times of 30 s per frame. Data integration, absorption, and Lorentz polarization corrections were made by the SAINT and SADABS subprograms in the SMART software packages.[20] Assignments of the space groups from the diffractometer data were made on the basis of the Laue symmetry and systematic absence analyses. Structure refinements were performed with the aid of the SHELXTL subprogram.[20]

Table 1. Crystal Data and Structure Refinement for $SrAu_{4.30(1)}In_{1.70(1)}$ (1) and $CaAg_{3.54(1)}In_{1.88(1)}$ (2)

formula	$SrAu_{4.30(1)}In_{1.70(1)}$	$Ca_{26.0(2)}Ag_{92.0(1)}In_{49.0(2)}$[a]
f.w.	1130.18	16592.3
space group/Z	*Pnma*/4	*P6/mmm*/1
unit cell (Å)		
a	9.102(1)	20.660(3)
b	5.6379(9)	20.660(3)
c	11.515(2)	9.410(2)
V (Å^3)/d_{cal} (g/cm^3)	590.9(2)/12.70	3478.4(10)/7.92
abs. coeff. (mm^{-1})	121.77	21.48
refl. coll./R_{int}	3530/0.0474	22038/0.0414
data/restr./para.	778/0/42	1713/2/98
GOF on F^2	1.245	1.14
R1/wR2 [$I > 2\sigma(I)$]	0.0584/0.1487	0.0375/0.0775
[all data]	0.0615/0.1499	0.0386/0.0787

[a] The formula, f.w., and d_{cal} values for **2** are different from those in cif file (Supporting Information) in which Cd is used to represent Ag/In mixtures in the structural solution.

Direct methods for **1** yielded six atoms: five had separations suitable for Au/In−Au/In pairs and the remaining one, for Sr−Au/In, so they were initially assigned to Au1−Au5 and Sr, respectively. Subsequent least-squares refinements proceeded smoothly and R1 converged at 13.7%. Examination of the resulting isotropic displacement parameters revealed that the assigned Au4 and Au5 had larger U_{eq} values (0.031 and 0.050 Å^2, respectively) compared with the other four atoms (0.015−0.022 Å^2), indicating that the former sites could be occupied by Au/In mixtures or pure In. Therefore, In4 and In5 were temporarily assigned to the former Au4 and Au5 atoms in subsequent refinements. At this stage, only In4 had an abnormal U_{eq} value (0.0089 Å^2) compared with those of other atoms (0.024−0.032 Å^2), indicating a Au/In mixture at this site. This was so assigned in the final anisotropic refinements, in which R values drastically decreased to R1 = 5.84%, wR2 = 14.87% for 42 variables and 735 independent reflections. The refined composition is $SrAu_{4.30(1)}In_{1.70(1)}$, consistent with the energy dispersive X-ray (EDX) data ($SrAu_{4.1(1)}In_{1.9(1)}$). The maximum and minimum peaks in the final difference Fourier map were 3.66 e$^-$/Å^3 (1.85 Å to Sr) and −4.04 e$^-$/Å^3 (1.55 Å to Au2), respectively.

Direct methods for **2** located 15 atoms, all with interatomic separations reasonable for Ag/In−Ag/In pairs (~ 2.8−2.9 Å), so Ag1−Ag15 were temporarily assigned to these sites. A few cycles of refinements resulted R1 = ~ 19%, and the difference Fourier map yielded four sites apparently suitable for polar Ca−Ag/In contacts (~ 3.2 Å). They were so assigned to Ca1−Ca4 in subsequent refinements, which converged at R1 = ~12%. At this stage, the difference Fourier map indicated two additional sites (Ag16 and Ag17) with smaller peaks and shorter distances to neighboring atoms. Ag16 was observed to be equivalent to Cd16 in the defect-free, structurally closely related $Na_{26}Cd_{141}$,[21] whereas Ag17 could be considered as part of a split site of Ag16 (below). Not surprisingly, both Ag16 and Ag17 had fractional occupancies and short distances to respective neighbors. Separate refinements to check the occupancies of Ag1−Ag15 and Ca1−Ca4 sites were also tried. The refined occupancy values for Ag1−Ag15 and Ca1−Ca3 were in the range of 0.98 (3)−1.02 (3), indicating full occupancies for these sites, but the occupancy for Ca4 was refined to 0.90(4). Additional refinements

dx.doi.org/10.1021/ic2016275 |*Inorg. Chem.* 2011, 50, 11091–11098

Table 2. Atomic Coordinates and Equivalent Isotropic Displacement Parameters for $SrAu_{4.30(1)}In_{1.70(1)}$ (1)[a]

atom	Wyck.	symm.	occ.	x	y	z	U_{eq} (Å^2)
Au1	4c	.m.		0.0701(2)	1/4	0.0857(2)	0.022(1)
Au2	4c	.m.		0.4047(2)	1/4	0.0177(2)	0.022(1)
Au3	4c	.m.		0.3158(2)	1/4	0.2637(2)	0.028(1)
Au/In	8d	1	0.65/0.35(2)	0.0630(2)	0.5131(3)	0.3038(2)	0.026(1)
In	4c	.m.		0.1447(4)	1/4	0.8603(3)	0.020(1)
Sr	4c	.m.		0.2588(5)	1/4	0.5590(4)	0.019(1)

[a] U_{eq} is defined as one third of the trace of the orthogonalized U_{ij} tensor.

Table 3. Atomic Coordinates and Equivalent Isotropic Displacement Parameters for $CaAg_{3.54(1)}In_{1.88(1)}$ (2)[a]

atom[b]	Wyck.	symm.	occ. ≠ 1	x	y	z	U_{eq} (Å^2)
M1	6l	mm2		0.1354(1)	0.2708(1)	0	0.017(1)
M2	12p	m..		0.1317(1)	0.4081(1)	0	0.016(1)
M3	12o	.m.		0.2608(1)	0.5216(1)	0.1558(1)	0.018(1)
M4	6j	m2m		0.4150(1)	0	0	0.022(1)
M5	12o	.m.		0.1803(1)	0.3607(1)	0.2515(1)	0.018(1)
M6	6j	M2m		0.1364(1)	0	0	0.032(1)
M7	12o	.m.		0.6161(1)	0.2323(1)	0.3338(1)	0.023(1)
M8	2c	−6m2		1/3	2/3	0	0.024(1)
M9	24r	1		0.1095(1)	0.4545(1)	0.2747(1)	0.024(1)
M10	6k	m2m		0.3884(1)	0	1/2	0.025(1)
M11	6m	mm2		0.5503(1)	0.1005(1)	1/2	0.025(1)
M12	6i	2mm		1/2	0	0.2497(2)	0.021(1)
M13	12q	m..		0.0876(1)	0.3156(1)	1/2	0.042(1)
M14	12o	.m.		0.0935(1)	0.1869(1)	2602(1)	0.045(1)
M15	6k	m2m		0.1523(1)	0	1/2	0.042(1)
M16	1a	6/mmm	0.31 (1)	0	0	0	0.025[c]
M17	2e	6mm	0.257(8)	0	0	0.091(1)	0.025[c]
Ca1	6l	mm2		0.5750(1)	0.1499(2)	0	0.020(1)
Ca2	12n	..m		0.2759(1)	0	0.2028(3)	0.021(1)
Ca3	6m	mm2		0.2393(1)	0.4786(2)	1/2	0.026(1)
Ca4	2e	6mm	0.90(4)	0	0	0.278(3)	0.084(8)

[a] U_{eq} is defined as one third of the trace of the orthogonalized U_{ij} tensor. [b] M = Ag, In, or Ag/In as they are indistinguishable in X-ray diffraction. [c] Fixed values in refinements.

were also tried with all Ag sites being assigned as In, but no significant change was observed judging from *R* values, U_{eq}, or other related parameters (e.g., residual peak heights) within our imagination because Ag and In are close in atomic number *Z*. However, attempts to assign Ag/In admixtures to different sites resulted in divergent refinements. Apparently, Ag and In are indistinguishable in this X-ray solution.

For the best approximation, Cd was used in the following least-squares refinements because it has the average atomic number of Ag and In. (The scattering coefficients of Cd are actually not an average of Ag and In, though.) Nevertheless, M will be used to represent the indistinguishable Ag/In mixtures in later text. The final refinements yielded R1 = 3.75%, wR2 = 7.87% for 102 variables and 1713 independent reflections. The refined composition was $Ca_{25.80(4)}Cd_{140.82(3)}$, a proportion very close to that of $Na_{26}Cd_{141}$. Since this was a pure phase product (Supporting Information, Figure S1), the formula for **2** is represented by the loaded ratio, $Ca_{26.0(2)}Ag_{92.0(1)}In_{49.0(2)}$ or, normalized, $CaAg_{3.54(1)}In_{1.88(1)}$, which agrees well with the EDX data.

As expected, the refinements of **2** could result in high residues in a difference Fourier map because of mismatches in X-ray scattering coefficients, which in turn might be mistakenly assigned to atoms with fractional occupancies. In this case, the maximum and minimum residual peaks are 8.64 e$^-$/Å^3 at (0 0 1/2) and −4.55 e$^-$/Å^3 at (0 0 0.207) sites, respectively. However, no meaningful electron densities were found at the corresponding sites in the observed Fourier map (Supporting Information, Figure S2). Large residues in the difference Fourier map were also reported in the structure of $Y_{13}Pd_{40}Sn_{31}$.[22]

Other arguable imperfections are the isotropic parameters for M6, M13−M15, and Ca4; all show considerably larger U_{eq} values than the average of other atoms. The reason is because M6, M14, and M15 define a hexagonal tunnel, in which the disordered M16 and M17 alternate with Ca4 along the *c* axis (Supporting Information, Figure S2). M13 is also affected by the disorder phenomena as it is coplanar with M15 on the waist of the hexagonal tunnel.

A summary of crystal and structural refinement data for both crystals is given in Table 1, and the refined positional parameters for **1** and **2** are given in Table 2 and Table 3, respectively, both standardized with TIDY.[23] Other detailed crystallographic data are available in the cif file (Supporting Information).

Electronic Structure Calculations. Electronic structure calculations were performed by the self-consistent, tight-binding, linear-muffin-tin-orbital (LMTO) method[24−26] in the local density (LDA) and atomic sphere (ASA) approximations, within the framework of the density

dx.doi.org/10.1021/ic2016275 |*Inorg. Chem.* 2011, 50, 11091–11098

functional theory (DFT) method.[27] Interstitial spheres were introduced to achieve space filling. The ASA radii as well as the positions and radii of these empty spheres were calculated automatically under the limitation of 16%, 18%, and 20% for atom−atom, atom-interstitial, and interstitial-interstitial sphere overlaps. Reciprocal space integrations were carried out using the tetrahedron method. The basis sets for Sr, Au, and In were 5s/(5p)/4d, 6s/6p/5d/(5f), 5s/5p/(5d); and for Na and Cd, 3s/(3p) and 5s/5p/4d/(4f). The orbitals in parentheses were down-folded in the calculations. Scalar relativistic effects were included in the calculations. The band structure was sampled for 8 × 8 × 8 k points for $Sr_3Au_{13}In_5$ and 12 × 12 × 4 for $Na_{26}Cd_{141}$ in the irreducible wedge of the Brillouin zone.

RESULTS AND DISCUSSION

Phases in Sr−Au−In System. Figure 1 shows the distribution of known ternary phases in the Sr−Au−In system; $SrAuIn_3$ ($I4mm$),[28] $SrAu_{1.06}In_{2.94}$ ($I4/mmm$),[29] $Sr_2Au_{2.85}In_{4.15}$ ($P\bar{6}2m$),[30] $Sr_4Au_9In_{13}$ ($P\bar{6}m2$),[31] $SrAu_{3.35}In_{4.65}$ ($P2_1/m$),[32] $SrAu_{3.76}In_{4.24}$ ($Pnma$),[31] SrAuIn ($Pnma$),[28] $SrAu_2In_2$ ($Pnma$),[33] and $SrAu_3In_3$ ($Pmmn$),[18] which are numbered from 1 to 9 in the figure. As shown, these phases aggregate in a region in which the valence electron count per atom (e/a) values fall within a range of 2.0−2.4. In contrast the present $SrAu_{4.3}In_{1.7}$ phase (red) lies in a lower e/a region, with e/a = 1.63. This e/a value is close to those of $Ca_3Au_{12.4}In_{6.1}$ (normalized as $CaAu_{4.1}In_{2.0}$), the 1/1 AC (1.73) in the Ca−Au−In system[14] and of $Ca_{13}Au_{57.1}Ga_{23.4}$ (normalized as $CaAu_{4.4}In_{1.8}$), the 2/1 AC (1.64) in the Ca−Au−Ga system.[13] The absence of QC/AC phases in Sr−Au−In system appears to have a relation with the larger size of Sr over Ca.

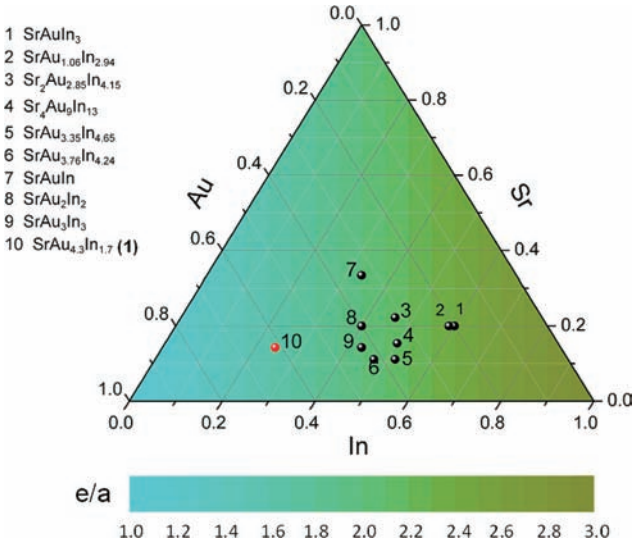

Figure 1. Distribution of ternary phases in the Sr−Au−In system. Black spheres denote phases reported in literature, and the red sphere denotes the phase discovered in present work. The color gradient of background is scaled by the valence electron count per atom (e/a), as indicated at bottom.

Crystal **1** has a very different structure motif. This is manifested by the building blocks and their arrangements. All other structures exhibit various hexagonal (or/and pentagonal) tunnels derived from $SrAuIn_3$ ($BaAl_4$-type)[18] except for the simplest SrAuIn.[28] Table 4 summarizes the coordination numbers of Sr versus (Au + In)/Sr proportions, as well as Au (at.) %, and e/a for all ternary phases. Generally, high coordination numbers are found for compounds with larger (Au + In)/Sr proportions.[31] This is because such large proportions mean that the electronegative components Au and In that define the networks around Sr need to be more condensed, resulting in the formation of more complex structures, as observed from SrAuIn[28] to $SrAu_2In_2$[33] and to $SrAu_3In_3$.[18] Crystal **1** has the largest coordination number (19) even though its (Au + In)/Sr proportion is not the largest. It seems that increases of Au atomic percentages, hence decreases of e/a, result in more compact structures with more delocalized and homogeneous covalent bonding.

Structure of $SrAu_{4.3}In_{1.7}$. $SrAu_{4.30(1)}In_{1.70(1)}$ ($oP28$), crystal **1**, is isostructural with the parent binary $CeCu_6$.[34] Other ternary

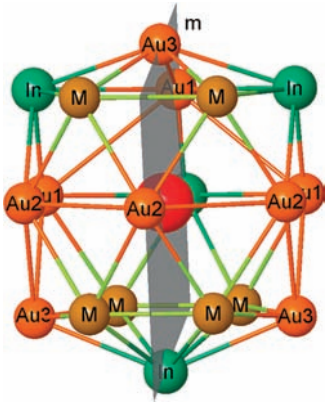

Figure 2. 19-Vertex polyhedron centered by Sr in $SrAu_{4.3}In_{1.7}$. (M = Au/In).

Table 4. Relationship between Sr Coordination Numbers versus (Au+In)/Sr Ratios, Au (at.) %, and e/a in Sr−Au−In Ternary Phases

phase	S. G.	(Au + In)/Sr	Au%	e/a	coordination numbers[a]	reference
SrAuIn	*Pnma*	2	0.33	2.00	12	28
$SrAuIn_3$	*I*4*mm*	4	0.20	2.40	16	28
$SrAu_{1.1}In_{2.9}$	*I*4/*mmm*	4	0.21	2.38	16	29
$Sr_2Au_{2.8}In_{4.2}$	*P*$\bar{6}$2*m*	3.5	0.32	2.14	16 + 15 + 13	30
$Sr_4Au_9In_{13}$	*P*$\bar{6}$*m*2	5.5	0.35	2.15	18, 16	31
$SrAu_{3.3}In_{4.7}$	*P*2$_1$/*m*	8	0.37	2.14	18	32
$SrAu_{3.8}In_{4.2}$	*Pnma*	8	0.42	2.05	18	31
$SrAu_2In_2$	*Pnma*	4	0.40	2.00	16	33
$SrAu_3In_3$	*Pmmn*	6	0.43	2.00	18	18
$SrAu_{4.3}In_{1.7}$	*Pnma*	6	0.61	1.63	19	this work

[a] The coordination numbers include only those with center-to-vertex distances <4.1 Å.

dx.doi.org/10.1021/ic2016275 |*Inorg. Chem.* 2011, 50, 11091–11098

Table 5. Selected Interatomic Distances for $SrAu_{4.30(1)}In_{1.70(1)}$ (1)[a]

bond		dist. (Å)	bond		dist. (Å)	bond		dist. (Å)
Au1	−Au2	3.144(3)	Au3	−M × 2	2.776(3)	In	−Au3 × 2	3.052(2)
	−Au3	2.893(3)		−M × 2	2.805(3)		−M × 4	2.988(4)
	−Au3	3.033(3)		−In × 2	3.052(2)		−M × 4	3.047(4)
	−M × 2	2.918(2)	M	−Au1	2.918(2)	Sr	−Au1 × 2	3.235(3)
	−In	2.682(4)		−Au2	2.817(2)		−Au1	3.287(5)
	−In × 2	3.487(2)		−Au2	2.916(3)		−Au2 × 2	3.223(3)
Au2	−Au3	2.946(3)		−Au3	2.805(3)		−Au2	3.342(5)
	−M × 2	2.817(2)		−Au3	2.776(3)		−Au3	3.440(5)
	−M × 2	2.916(3)		−M	2.671(4)		−M × 2	3.516(5)
	−In	2.980(4)		−M	2.967(4)		−M × 2	3.585(5)
	−Au1	3.144(3)		−In	2.988(4)		−In	3.621(4)
	−Au2 × 2	3.335(3)		−In	3.047(4)		−In	3.633(4)
Au3	−Au1	2.893(3)	In	−Au1	2.682(4)		−Au3 × 2	3.736(3)
	−Au1	3.033(3)		−Au1	3.487(2)		−M × 2	3.743(5)
	−Au2	2.946(3)		−Au2	2.980(4)		−In × 2	3.735(4)

[a] M = 0.65(2) Au + 0.35 (2) In.

phases with the same structural type are usually found as RCu_5M (R = rare-earth metals, M = In or Sn);[35−37] some pseudo binaries have also been reported, for example, $CeCu_{6-x}Au_x$.[38] The building block for the present structure type is the active-metal-centered 19-vertex polyhedral cluster $Sr@Au_9In_4M_6$ (M = Au/In), Figure 2. The cluster consists of pentagonal and hexagonal caps, with a hexagonal ring waist. The whole cluster exhibits mirror plane symmetry perpendicular to the vertical *b* axis, as shaded. The distances between the two equivalent, parallel quadrangular planes (Au1 → Au3 → Au2 → In) equal the lattice parameter *b*. Nineteen Sr−Au, Sr−In, and Sr−M distances in this cluster are within 3.24−3.74 Å, Table 5, whereas those in the second sphere are much further away, > 5.2 Å. The bond distances for Au−Au, Au−In, Au−M, In−M, and M−M are comparable with the sum of single bond metallic radii (Au, 1.339; In, 1.421[39]), except that d_{Au1-In} is shorter than expected, 2.682 (4) Å. A similar distance is found in $Sr_4Au_9In_{13}$ (2.66 Å)[31] and is explained by the smaller number of neighbors about each. The same reason applies to **1**, see Table 5.

The 19-vertex clusters are rarely seen in other structure types; rather, 18- or 20-vertex clusters are more common. For examples, 20-vertex dodecahedral clusters are often found in Zintl phases containing heavier triels (Ga, In, Tl).[6] From the viewpoint of geometry, the $Sr@Au_9In_4M_6$ cluster in **1** vividly mimics the 18-vertex clusters in $Ca_3Au_{12.4}In_{6.1}$ (YCd_6-type),[14] except that the latter contains two pentagonal caps and a hexagonal ring at the waist. Apparently, the increase of coordination number from Ca to Sr is required by size; the larger Sr evidently needs more anionic neighbors to achieve space filling.

Each unit cell of $SrAu_{4.3}In_{1.7}$ consists of four $Sr@Au_9In_4M_6$ clusters, two at *y* = 0.25 and two at *y* = 0.75, Figure 3. These polyhedra share the M_2In triangle faces with each other in (101) and (011) directions. In the (010) direction, each polyhedron shares its quadrangular planes (Au1 → Au3 → Au2 → In) with other two polyhedra to form a polyhedral column along *b*, see Figure 3 b. The structure can also be considered as a pseudo layered structure along the *b* axis: "$SrAu_3In$" layers at $y = {}^1/_4$ and ${}^3/_4$ plus M layers between. This is evident in the *y* coordinates in Table 2. However, the mixed Au/In form strong bonds with atoms from neighboring "$SrAu_3In$" layers, particularly the bonding interactions

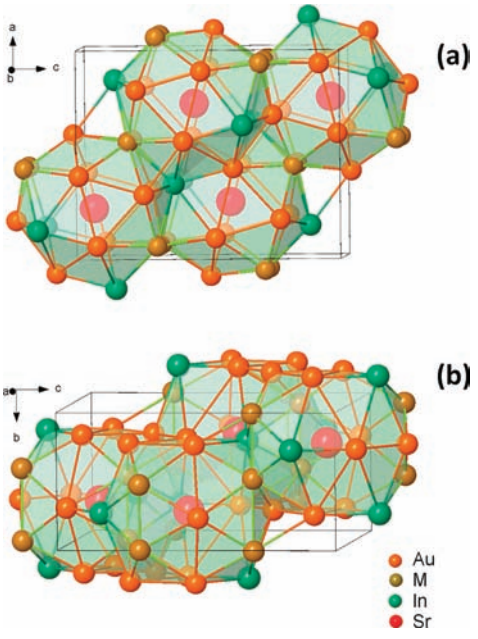

Figure 3. Packing of the 19-vertex polyhedral clusters in the unit cell of $SrAu_{4.3}In_{1.7}$ viewed along (a) [010] and (b) [100] directions.

with Au as suggested by their bond distances d_{M-Au} = 2.776−2.918 Å, Table 5, diminishing the layered structural features.

Structure of $CaAg_{3.6}In_{1.9}$. The structure of $CaAg_{3.6}In_{1.9}$, crystal **2**, is related to both $Na_{26}Cd_{141}$ (*hP*167)[21] and $Y_{13}Pd_{40}Sn_{31}$ (*hP*168),[22] which have the same space group (*P6/mmm*) and are free of any detectable defects. Both prototypes contain four independent sites for active metals (Na or Y) and 16 sites for electronegative components. Their differences lie mainly in two crystallographic sites: in $Y_{13}Pd_{40}Sn_{31}$, the Wyckoff 1*b* (0 0 0) site is empty but the Wyckoff 2*d* (1/3 2/3 1/2) site is occupied by a Sn atom (Sn1). In contrast, a Cd atom (Cd16) is assigned to the 1*b* site with nothing at 2*d* in $Na_{26}Cd_{141}$. As a result, $Y_{13}Pd_{40}Sn_{31}$ contains one more atom in the unit cell compared with $Na_{26}Cd_{141}$. The

dx.doi.org/10.1021/ic2016275 |*Inorg. Chem.* 2011, 50, 11091–11098

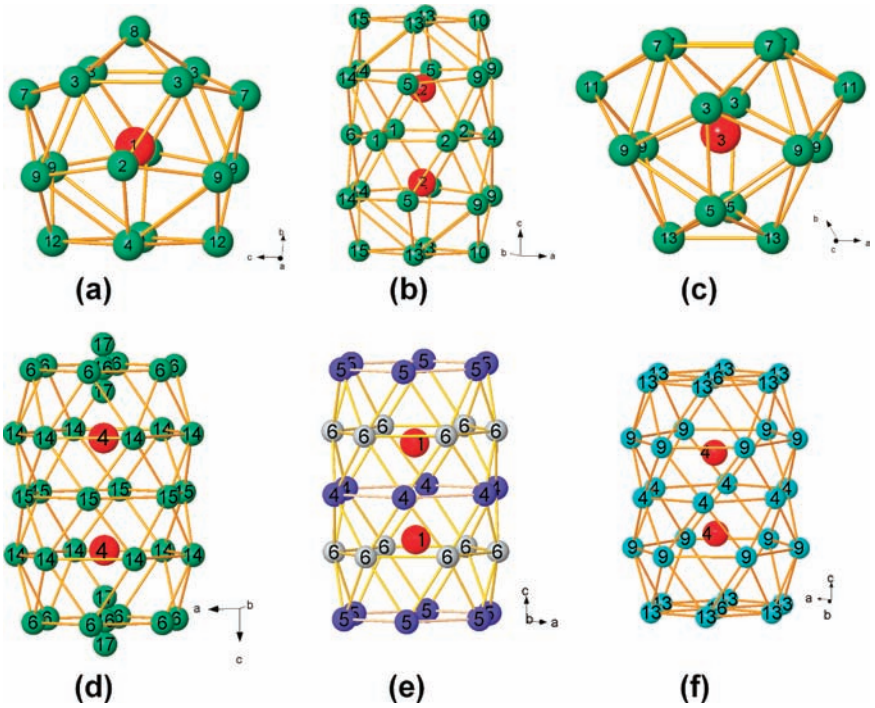

Figure 4. Environments of Ca1−Ca4 (a−d) in $CaAg_{3.5}In_{1.9}$ (**2**), together with the structurally related (e) Y1-cluster in $Y_{13}Pd_{40}Sn_{31}$ and (f) Na4-cluster in $Na_{26}Cd_{141}$. Red and green spheres in (a−d) represent Ca and Ag/In atoms, as listed in Table 3. Violet, gray, red in (e) represent Pd, Sn, and Y, and cyan and red in (f), Cd and Na, respectively.

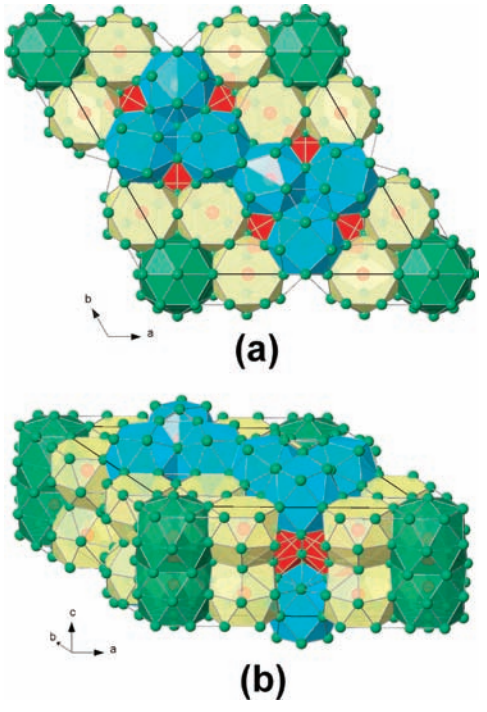

Figure 5. Polyhedral representations of the structure of $CaAg_{3.5}In_{1.9}$ projected in (a) (001) and (b) ~(010) directions. Blue, yellow, red, and green represent Ca1, Ca2, Ca3, and Ca4-centered polyhedra, respectively.

structure of crystal **2** is closer to $Na_{26}Cd_{141}$, with the Wyckoff 1*b* sites occupied by M16 (M = Ag/In) but the 2*d* site unoccupied. However, the M16 site exhibits configurational disorder with M17 (below).

Figure 4 a−d show the coordination polyhedra of Ca1−Ca4, together with the polyhedra from $Y_{13}Pd_{40}Sn_{31}$ (e) and $Na_{26}Cd_{141}$ (f). Each Ca1 has 17 neighbors that define pentagonal prisms with all faces capped. In comparison, both Ca2 and Ca3 have 16 neighbors, which define a pentagonal prism similar to those around Ca1 except that one rectangle face (1→1→2→2 for Ca2 and 7→7→7→7 for Ca3) on the waist is uncapped. Note that the 1→1→2→2 open rectangular face for Ca2 happens to be coplanar with two neighboring capping atoms (M4 and M6) to generate a hexagonal face. The last is shared with another Ca2 polyhedron. That is, two neighboring Ca2 polyhedra pair up to form a dimer, Figure 4 c, with the Ca2−Ca2 distance about 3.33 Å. This reminds one of the similar Ca_2 dimers in $Ca_{14}Au_{46}Sn_5$,[17] $Ca_{13}Au_{57.1}Ga_{23.4}$,[13] and $Ca_{12.6}Au_{37.0}In_{39.6}$,[14] all of which have short Ca−Ca distances (<3.5 Å).

The coordination polyhedron about Ca4, Figure 4d, includes marked configurational disorder, different from those of Ca1−Ca3. To clarify its structural feature, let us first examine the closely related defect-free clusters $(Y1)_2@Pd_{12}Sn_{18}$ in $Y_{13}Pd_{40}Sn_{31}$[24] and $(Na4)_2@Cd_{32}$ in $Na_{26}Cd_{141}$.[22] As shown in Figure 4e, each Y1 is surrounded by a hexagonal drum defined by 6 Sn4, 6 Sn5, and 6 Pd6 atoms, with the last in the waist. Because Y1 is slightly off the center of the drum and shifted toward the $(Sn4)_6$ face, two neighboring drums appear as a dimer sharing the common $(Sn4)_6$ hexagonal face. The dimeric drums stack with each other through shared $(Sn5)_6$ faces, forming infinite hexagonal columns extending along *c*. The corresponding Na4-polyhedra in $Na_{26}Cd_{141}$, Figure 4f, exhibit a similar structural motif except that the face centers of $(Cd13)_6$ hexagonal faces are occupied by Cd16 atoms. The Ca4-polyhedra in **2** are similar to (f) except that each fractional M16 is accompanied by two fractional M17, disordered above and below in *c* with short distance of $d_{M16\text{-}M17} \approx 0.87$ Å. The disorder at these sites will be discussed below.

dx.doi.org/10.1021/ic2016275 |*Inorg. Chem.* 2011, 50, 11091–11098

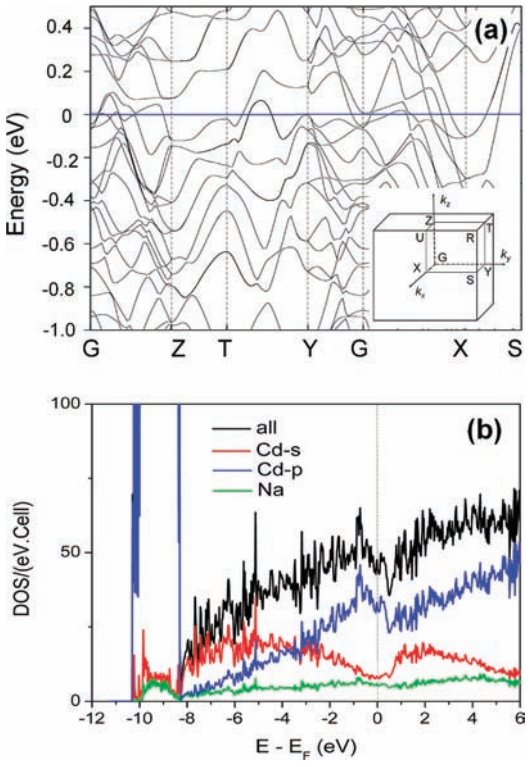

Figure 6. (a) Band structure of the hypothetical $Sr_3Au_{13}In_5$ (*Pnma*), a 1 × 3 × 1 superlattice of $SrAu_{4.3}In_{1.7}$. (b) The density-of-states (DOS) for $Na_{26}Cd_{141}$, a structure closely related to that of $CaAg_{3.5}In_{1.9}$.

The arrangements of these four types of clusters in **2** are very complex. Cenzual and Parthé have described this type of structure as an intergrowth structure containing segments of $CaAu_5$, $MnCu_2Al$, and the W structures.[22] But it is more convenient here to discuss the structure in terms of the four different clusters mentioned above. As shown in Figure 5a, three Ca1 clusters (blue) aggregate into a triad through sharing the common vertex M8, which is located at Wyckoff 2*c* (1/3 2/3 0) special position. Each triad shares its (M12→M4→M12→M4) faces with other three triads in the same layer to generate a two-dimensional Ca1-polyhedral layer. Similarly, three neighboring Ca3-polyhedra (red) also form a triad, with the uncapped 7→7→7→7 rectangle faces form a trigonal prism. The equivalent prism in $Y_{13}Pd_{40}Sn_{31}$ is centered by Pd1 at Wyckoff 2*d* (1/3 2/3 1/2). The Ca3-triads are discrete without other linkages in the structure, in contrast to the Ca1-triads. All Ca3-triads are located in the z = 1/2 layer, as if sandwiched by Ca1-polyhedral layers, Figure 5b. Such an assembly of Ca1- and Ca3-triads leaves hexagonal cavities, which are filled by Ca2- (yellow) and Ca4-polyhedra (green), with the latter at the origin.

Disorder in $CaAg_{3.5}In_{1.9}$. If M17 is disregarded, M16 would have an elongated tensor in *c* (U_{11}: U_{22}: U_{33} = 0.022: 0.022: 0.986) in the refinements with anisotropic displacement parameters. Apparently, M17 should be considered as the split sites of M16. In other words, M16 disorders by moving up and down to M17 sites along *c*. As a consequence, Ca4 can also slightly shift from its center along *c*, as indicated by its displacement parameters (U_{11}: U_{22}: U_{33} = 0.032: 0.032: 0.189). Therefore, the disorder between M16/M17 and Ca4 is a synergistic response to each other. It resolves the problem incurred from the unphysical short distance $d_{Ca4-M16} \approx 2.62$ Å, so the structure can be viewed as an average of many unit cells in which the M16 and Ca4 are continuously disordered, c.f. Supporting Information, Figure S3. Positional disorders (splits) are commonly seen in tunnel-like environments such as in $K_{0.4}Cd_2$,[21] $K_xAu_4In_2$,[40] and $K_xAu_2In_2$.[41] In some cases, the disorders are strong enough to yield superlattice, commensurate, or incommensurate reflections, for example, in $Sc_4Mg_xCu_{15-x}Ga_{7.5}$.[8] However, this was not verified for the present data set. Varied low-temperature X-ray single crystal diffractions would be interesting for further analyses.

Electronic Structure. *$SrAu_{4.3}In_{1.7}$.* Apparently, special treatments need to be made to circumvent the Au/In mixture at the 8*d* site in **1**. This was done by the construction of a superstructure model, $Sr_3Au_{13}In_5$, in the same space group but with a tripled lattice *b*. In this way, three independent sites corresponding to the 8*d* site in the parent structure were generated, and one was assigned to In and the other two to Au since the Au/In ratio is 0.65/0.35 ≈ 2/1. This leads to three different colorings, and the results for the model with lowest total energy are discussed here.

Figure 6a shows the band structure of the hypothetical $Sr_3Au_{13}In_5$ around Fermi energy (E_F). The Fermi level crosses many dispersed bands, suggesting a metallic character for this phase. The band crossings result in the formation of a complex Fermi surface with wrapped holes and pockets, which makes the structure unlikely to be destabilized by small composition variations, consistent with our experimental observations (above). The Sr 4d states (not shown) are mainly populated in the conduction band, but a small number of states at lower energy are found to interact with s and p states of Au and In, a scenario similar to that of Ca in $CaAu_{4.1}In_2$ and other intermetallics.[13−16] As mentioned, although the structure appears to show layers at z = $^1/_4$ and $^3/_4$, the strong M−Au and M−In bonds change the layers into three-dimensional frameworks. Therefore, the band structure does not show anisotropic properties, Figure 6. Rather, the bands in the G → Z and G → X directions that are associated with the *ac* plane in the first Brillouin zone and those in the G → Y and Z → T directions along the *b* axis are almost equally dispersed.

$Na_{26}Cd_{141}$. Because of the presence of configurational disorder in $CaAg_{3.5}In_{1.9}$, the electronic structure of alternative $Na_{26}Cd_{141}$ is discussed. This should give a general knowledge on the electronic structure of $Ca_{26}Ag_{92}In_{49}$ because the structures are very similar and the electronic configurations of Ag and In are similar to that of Cd. The total density-of-states (DOS) of $Na_{26}Cd_{141}$, Figure 6b, is a continuous curve crossing the Fermi energy, the signature of a metal. The total DOS is dominated by Cd states, with s states mainly in the low energy region and p states around the Fermi level. The profile of total DOS appears to be a free-electron-like system inasmuch as the core-like Cd d states (−10.3 to −8.3 eV) have negligible contributions. However, the Fermi level is found on a declining slope of DOS, confirming its location in a pseudogap.

The occurrence of pseudogaps is a common feature for Hume−Rothery phases, in which the matching between Fermi surface (FS) and certain sizable Brillouin zones (BZ) results in a sharp drops in DOS because of the sudden increase of available space for electrons via FS−BZ interactions.[4] As a result, Hume−Rothery phases appear to converge at certain valence electron counts (vec) or their averages (e/a). For example, e/a for γ brass phases is ∼1.62,[3] and for a Tsai-type QC, ∼ 2.0.[4] However, a similar mechanism could not be established in the present system, disregarding the fact that the Ag d states could hide the free-electron feature in DOS in a real situation. Pseudogaps could also suggest some other interactions dictated by composition, structure, bonding, or their combinations that occur at

dx.doi.org/10.1021/ic2016275 |*Inorg. Chem.* 2011, 50, 11091–11098

the Fermi energy. Judging from the partial DOS, s-p mixings of Cd could be the major reason. However, it is unclear whether Ca d states in **2** would enhance the depth of the pseudogap or not, although they do so in the Ca−Au−M (M = Ga, In) 1/1 ACs.[13,14] (Calculations on the hypothetical $Ca_{26}Cd_{141}$ were not feasible because of limitations in the number of orbitals in the computer/software. This was the same reason for LMTO calculations on $Na_{26}Cd_{141}$ about 10 years ago.[21])

REMARKS

Both $SrAu_{4.3}In_{1.7}$ and $CaAg_{3.5}In_{1.9}$ have the smallest e/a values (1.63 vs 1.74) among all known phases in the respective systems, thanks to the large amounts of Au and Ag components. The two phases exhibit diversified polyanionic networks in which some building units mimic those found in $CaAu_4In_2$, an AC phase. It appears that intermetallic phases in such low e/a region are sensitive to both atomic size and certain e/a ranges.

Finding QCs and approximants following the fruitful $CaAu_4M_2$ (M = Ga, In, Ge, Sn) series may be impossible when the active metal Ca is replaced by Sr, as exemplified by $SrAu_{4.3}In_{1.7}$. Although no parallel experiments were tested with other larger active metals with empty low-lying d orbitals (K, Rb, Cs, Ba, etc.), one is unlikely to find QC/ACs with these because higher coordination numbers are required in space filling, as exemplified by $SrAu_{4.3}In_{1.7}$. The replacement of electronegative Au by Ag, with slightly larger size but a smaller relativistic effect, produces mainly the hexagonal phase $CaAg_{3.5}In_{1.9}$ in the same phase field. However, a 2/1 AC phase evidently remains in the electron rich region ("$CaAg_3In_3$") in this system,[19] and a QC phase has also been reported at $Ca_{16}Ag_{42}In_{42}$.[42] This illustrates that a relativistic effect as large as that of Au is not necessary in QC formation. However, the large relativistic effect of Au enables greater alloying with In or other metals compared with Ag, making e/a of some phases containing Au smaller than that of Ag. For example, $CaAu_{4.1}In_2$ (e/a = 1.73)[14] versus $CaAg_2In_4$ (2.29),[43] both in $Im\bar{3}$. Nevertheless, both examples in this work demonstrate that size factors play critical roles in the QC/AC formation. So, efforts to search for new QC/ACs should probably avoid Sr or larger active metals, but replacement of Au with other late transition metals (Ag, Pd, Pt, etc.) remains open.

ASSOCIATED CONTENT

Supporting Information. The experimental powder patterns in Figures S1, observed electron densities in Figure S2, the schematic disorder patterns in Figure S3, and cif data. This material is available free of charge via the Internet at http://pubs.acs.org.

AUTHOR INFORMATION

Corresponding Author
*E-mail: jcorbett@iastate.edu.

ACKNOWLEDGMENT

A reviewer's comments on the dispersion of bands in Figure 6a and the observed electron density map (Supporting Information, Figure S2) were very helpful. This research was supported by the U.S. National Science Foundation, Solid State Chemistry, via Grant DMR-0853732. All of the work was performed in the facilities of the Ames Laboratory, U.S. Department of Energy.

REFERENCES

(1) Corbett, J. D. *Inorg. Chem.* **2010**, *49*, 13.
(2) Hume-Rothery, W. *J. Inst. Met.* **1926**, *35*, 295.
(3) Hume-Rothery, W.; Raynor, G. V. *The Structure of Metals and Alloys*, 4th ed.; Institute of Metals: London, U.K., 1962.
(4) Mizutani, U. In *The Science of Complex Alloy Phases*; Massalski, T. B., Turchi, P. E. A., Eds.; TMS (The Minerals, Metals & Materials Society): Warrendale, PA, 2005; pp 1−42.
(5) Lin, Q.; Corbett, J. D. *Struct. Bonding (Berlin)* **2009**, *133*, 1.
(6) Kauzlarich, S. M., Ed.; *Chemistry, Structure, and Bonding of Zintl Phases and Ions*; VCH: New York, 1996.
(7) Miller, G. J.; Lee, C.-S.; Choe, W. In *Inorganic Chemistry Highlights*; Meyer, G., Naumann, D., Wesemann, L., Eds.; Wiley-VCH: Weinheim, Germany, 2002; pp 21−53.
(8) Lin, Q.; Lidin, S.; Corbett, J. D. *Inorg. Chem.* **2008**, *47*, 1020.
(9) Lin, Q.; Corbett, J. D. *Inorg. Chem.* **2005**, *44*, 512.
(10) Lin, Q.; Corbett, J. D. *Inorg. Chem.* **2007**, *46*, 8722.
(11) Lin, Q.; Corbett, J. D. *Inorg. Chem.* **2009**, *48*, 5403.
(12) Lin, Q.; Corbett, J. D. *Inorg. Chem.* **2008**, *47*, 3462.
(13) Lin, Q.; Corbett, J. D. *Inorg. Chem.* **2008**, *47*, 7651.
(14) Lin, Q.; Corbett, J. D. *J. Am. Chem. Soc.* **2007**, *129*, 6789.
(15) Lin, Q.; Corbett, J. D. *Inorg. Chem.* **2010**, *49*, 4570.
(16) Lin, Q.; Corbett, J. D. *Inorg. Chem.* **2010**, *49*, 10436.
(17) Lin, Q.; Corbett, J. D. *Inorg. Chem.* **2011**, *50*, 1808.
(18) Muts, I. R.; Schappacher, F. M.; Hermes, W.; Zaremba, V. I.; Poettgen, R. *J. Solid. State Chem.* **2007**, *180*, 2202.
(19) The powder pattern of "$CaAg_3In_3$" can be completely indexed by a primitive cubic cell, with a = 24.952 (1) Å, about τ (= 1.618) times that of $CaAg_2In_4$ (a = 15.454 Å), the 1/1 AC of of $Ca_{16}Ag_{42}In_{42}$ QC.[42] Apparently, this phase is the corresponding 2/1 AC.
(20) *SHELXTL*; Bruker AXS, Inc: Madison, WI, 2000.
(21) Todorov, E.; Sevov, S. C. *Inorg. Chem.* **1998**, *37*, 6341.
(22) Cenzual, K.; Parthe, E. *Acta Crystallogr., Sect. C* **1984**, *40*, 1127.
(23) Gelato, L. M.; Parthé, E. *J. Appl. Crystallogr.* **1987**, *20*, 139.
(24) Shriver, H. L. *The LMTO Method*; Springer-Verlag: Berlin, Germany, 1984.
(25) Anderson., O, K.; Jepsen, O. *Phys. Rev. Lett.* **1984**, *53*, 2571.
(26) Jepsen, O.; Snob, M. *Linearized Band Structure Methods in Electronic Band-Structure and its Applications, Springer Lecture Notes*; Springer Verlag: Berlin, Germany, 1987.
(27) Tank, R.; Jepsen, O.; Burkhardt, A.; Andersen, O. K. *TB-LMTO-ASA Program*, Vers. 4.7; Max-Planck-Institut für Festkörperforschung: Stuttgart, Germany, 1994.
(28) Muts, I. R.; Poettgen, R.; Zaremba, V. I. *Z. Anorg. Allg. Chem.* **2007**, *633*, 2591.
(29) Tkachuk, A. V.; Mar, A. *Inorg. Chem.* **2007**, *180*, 2298.
(30) Hoffmann, R. D.; Poettgen, R.; Rosenhahn, C.; Mosel, B. D.; Kuennen, B.; Kotzyba, G. *J. Solid State Chem.* **1999**, *145*, 283.
(31) Palasyuk, A.; Dai, J. C.; Corbett, J. D. *Inorg. Chem.* **2008**, *47*, 3148.
(32) Palasyuk, A.; Maggard, P. A. *J. Alloys Compd.* **2010**, *491*, 81.
(33) Dai, J. C.; Corbett, J. D. *Inorg. Chem.* **2007**, *46*, 4592.
(34) Cromer, D. T.; Larson, A. C.; Roof, R. B. *Acta Crystallogr.* **1960**, *13*, 913.
(35) Zaremba, V.; Hlukhyy, V.; Stepen' Damm, Y.; Troc, R. *J. Alloys Compd.* **2001**, *321*, 97.
(36) Bobev, S.; Bauer, E. D. *Acta Crystallogr., Sect. E* **2005**, *61*, i89.
(37) Bobev, S.; Bauer, E. D. *Acta Crystallogr., Sect. E* **2005**, *61*, i79.
(38) Ruck, M.; Portisch, G.; Schlager, H. G.; Sieck, M.; Loehneysen, H. V. *Acta Crystallogr., Sect. B* **1993**, *49*, 936.
(39) Pauling, L. *The Nature of the Chemical Bond*, 3rd ed.; Cornell University Press: Ithaca, 1960; p 403.
(40) Li, B.; Corbett, J. D. *J. Am. Chem. Soc.* **2006**, *128*, 12392.
(41) Li, B.; Corbett, J. D. *J. Am. Chem. Soc.* **2005**, *127*, 926.
(42) Guo, J. Q.; Tsai, A. P. *Philos. Mag. Lett.* **2002**, *82*, 349.
(43) Sysa, L. V.; Kal'ichak, Y. M.; Galadzhun, Y. V.; Zaremba, V. I.; Aksel'rud, L. G.; Skolozdra, R. V. *J. Alloys Compd.* **1998**, *266*, 17.